Article:
Barlow, D., Goffrey, T., Bennett, K. et al. (11 more authors) (2022) Role of hot electrons in shock ignition constrained by experiment at the National Ignition Facility. Physics of Plasmas. 082704. ISSN 1089-7674

https://doi.org/10.1063/5.0097080

Role of Hot Electrons in Shock Ignition Constrained by Experiment at the National Ignition Facility

D. Barlow,[1,2] T. Goffrey,[1] K. Bennett,[1] R.H.H. Scott,[3] K. Glize,[3] W. Theobald,[4] K. Anderson,[4] A.A. Solodov,[4] M.J. Rosenberg,[4] M. Hohenberger,[5] N.C. Woolsey,[2] P. Bradford,[2] M. Khan,[2] and T.D Arber[1]

[1)] *Department of Physics, University of Warwick, Coventry, CV4 7AL, UK*

[2)] *York Plasma Institute, Department of Physics, University of York, York, YO10 5DQ, UK*

[3)] *Central Laser Facility, STFC, Rutherford Appleton Laboratory, Harwell, Oxford, OX11 0QX, UK*

[4)] *Laboratory for Laser Energetics, University of Rochester, Rochester, New York 14623-1299, USA*

[5)] *Lawrence Livermore National Laboratory, Livermore, California 94550, USA*

(*Electronic mail: Duncan.Barlow@u-bordeaux.fr)

(Dated: 25 July 2022)

Shock ignition is a scheme for direct drive inertial confinement fusion that offers the potential for high gain with the current generation of laser facility, however the benefits are thought to be dependent on the use of low adiabat implosions without laser-plasma instabilities reducing drive and generating hot electrons. A National Ignition Facility direct drive solid target experiment was used to calibrate a 3D Monte-Carlo hot electron model for 2D radiation-hydrodynamic simulations of a shock ignition implosion. The $\alpha = 2.5$ adiabat implosion was calculated to suffer a 35% peak areal density decrease when the hot electron population with temperature $T_h = 55$keV, and energy $E_h = 13$kJ was added to the simulation. Optimizing the pulse shape can recover $\sim 1/3$ of the peak areal density lost due to a change in shock timing. Despite the harmful impact of laser-plasma instabilities, the simulations indicate shock ignition as a viable method to improve performance and broaden the design space of near ignition high adiabat implosions.

I. INTRODUCTION

Shock ignition (SI)[1–7] is a potential high gain approach to direct drive inertial confinement fusion (ICF)[8–10]. Gain is the ratio of released fusion energy to input laser energy and is a key indicator of whether a method is suitable for energy generation. Direct drive ICF uses laser ablated material to drive a deuterium-tritium ice shell toward its gas filled core. For conventional hotspot ignition the inertia of the capsule wall must provide both the energy required for fusion and the confinement of the hotspot for the tens of picoseconds necessary to achieve thermonuclear burn. SI separates the assembly of the hotpot from the ignition energy requirement. The implosion is carried out below the self ignition velocity due to a less energetic assembly pulse, and a late-stage shock introduces the additional energy required to ignite the hotspot. The ignition shock collides with an outward travelling shock created by the reflection of the first shocks at the centre. The shock collision, if timed accurately, provides the increase in hotspot density and temperature required for ignition. The benefit of this method is that it exhibits the potential for high gain at lower laser energies[4] but it also opens up the ignition design space to lower velocity implosions that have been demonstrated to be more stable to hydrodynamic instabilities[11]. This is significant since hydrodynamic instabilities have been one of the major limiting factors on the success of ICF. For simulated high gain, laser driven implosions rely on either large target mass (and large laser energies) or near adiabatic compression (measured by shell adiabat[10]). The failure of the low adiabat ($\alpha < 2$) implosions to perform as simulated[12], has led the laser driven ICF community to develop higher adiabat ($\alpha > 3$) implosions. High adiabat implosions have led to better agreement with simulation enabling the incremental improvements for both indirect drive[13,14] and direct drive[15] approaches to the point where hydrodynamically scaled results are close to ignition (at $\simeq 1.8$MJ). While SI may lead to modest improvements in implosion performance at $\alpha > 2$ seen in Trela *et al.* [16] and Anderson *et al.* [17], it also introduces the significant unknown of a high intensity laser pulse. For 3rd harmonic Nd:glass lasers at 351nm (this wavelength is used throughout the rest of the paper) the laser intensity exceeds the $\sim 10^{15}\mathrm{W/cm^2}$ limit where laser-plasma instabilities (LPI) are thought to play an increasingly dominant role in laser absorption[18]. LPI have two significant impacts on the hydrodynamics of an implosion: reduced drive efficiency due to scattered light and the generation of hot electrons.

At intensities, $< 10^{15}\mathrm{W/cm^2}$, implosion dynamics from experiments have been matched in simulations, using semi-empirical multipliers to account for LPI scattered light, and hot electron preheat[19]. For the targets investigated in Christopherson *et al.* [19] it was found that hot electron preheat led to an increase in adiabat of $10-20\%$ and a reduction in stagnation areal density of $10-40\%$.

Simulation of hot electrons at SI relevant intensities ($> 10^{15}\mathrm{W/cm^2}$) have shown conflicting results[20,21]. Initially, for SI it was predicted that hot electrons have a negligible impact and in fact may improve drive efficiency due to their penetration depth[7,22]. Experiments appear to support this hypothesis, demonstrating the generation of strong shocks in the presence of LPI generated hot-electron populations[5,23,24]. Due to the hot electron drive efficiency, the idea of electron shock ignition was also theorized[21] where the aim of the final laser pulse is to maximize hot-electron generation from LPI. However, kinetic modelling of hot electrons using a simplified LPI

model embedded in a hydrodynamics simulation indicated that the production of hot electrons was found to be harmful to the implosion performance[20,25,26]. The deleterious effect of preheat[27] outweighs the benefit of drive support for hot electrons with a population temperature higher than 30keV or mono-energetic hot electron populations with an energy exceeding $\sim$ 50keV (target dependant). Conversely, there is evidence that kinetically modelled hot-electrons can provide benefit to implosion performance across a broad range of population temperatures[28–30] (up to 70keV). Within these simulations the LPI scattered light energy fraction is not explicitly related to the LPI hot-electron energy fraction which may explain the difference in impact of hot electrons compared to those that use simplified LPI models.

There are several hydrodynamic factors that may change the impact of hot electrons. Christopherson *et al.* [19] show that preheat is worse for lower adiabat implosions, and Colaïtis *et al.* [20] demonstrates that the inclusion of an ablator can help to reduce the penetration (thus preheat) of the hot electrons. Trela *et al.* [16] and Bel'kov *et al.* [31] demonstrate that the timing of the high-intensity spike can also change the amount of hot-electron preheat. The target and laser pulse shape design might be key to determine whether hot electrons have a harmful or beneficial effect to SI.

Even if a specific target and laser pulse shape is considered, there is still significant uncertainty over the LPI and the hot electron population generated. Fully kinetic simulations (such as PIC codes) are too expensive to run for the durations required to understand the LPI over a nanosecond pulse. Linear LPI theory does not include the non-linear interaction of many laser-plasma waves with non-thermal particle distributions at a range of densities. Despite these complexities there is evidence, from experiment[27,32] supported by PIC simulation[33], that stimulated Raman scattering (SRS) off plasma at $10-25\%$ of the critical density is the dominant LPI and source of hot electrons in the $> 3\times10^{15}\mathrm{W/cm^2}$ intensity regime.

In addition to difficulties with theory and simulation at SI relevant conditions, there is not a consensus in observation from experiment on hot electron characteristics. It is possible to use planar or conical geometry targets on lower energy facilities to increase laser intensity and make plasma conditions more closely map to those expected during SI implosions[34–40]. This is done to investigate the LPI and hot electrons that are generated at $> 10^{15}\mathrm{W/cm^2}$ intensities, long density scale lengths $\simeq 500\mu$m and electron temperatures $\simeq$ 3keV predicted to occur in SI plasmas[18,27]. Recent experiments conducted in planar or conical geometry at the Omega Facility[41,42] have attempted to infer the fraction of laser energy converted to hot electrons (η) and the temperature of the population (T_h)[32,43,44]. Zhang *et al.* [43] uses a planar target and predicts $\eta < 0.01$ in $T_h \simeq$ 30keV. Tentori *et al.* [44] also uses a planar target but predicts $\eta \simeq 0.10$ in $T_h \simeq$ 30keV. Scott *et al.* [32] uses a conical target and predicts $\eta \simeq 0.025$ in $T_h \simeq$ 45keV. The discrepancies are significant as the population is at the edge of what will cause acceptable preheat for SI[45]. There are many possible explanations for the differences, nonetheless it limits our ability to make predictions for SI implosions.

There are two additional aspects which are not well characterised by experiments or simulation, these are hot electron refluxing and emission angle (Ω_h). Hot electron refluxing occurs when the accumulated charge on a target prevents the escape of the electrons. An analysis of implosion capsule charging was presented in Sinenian *et al.* [46] and Volpe *et al.* [47] with MeV scale charge. Reflux information extracted from planar and conical targets might not be relevant to implosions due to the difference in target geometry, but the planar target experiment in Pisarczyk *et al.* [48] demonstrates similar accumulation of charge with electrons refluxed up to MeV energy scales. The refluxing hot electrons are expected to lead to additional coronal heating[49]. The most significant experimental constraint on hot electron emission angle can be seen in Yaakobi *et al.* [50] where the population is inferred to have a solid angle of $\Omega_h > 2\pi$ sr. PIC simulation and LPI theory give a much narrower angle, $\Omega_h \simeq 1.8$sr[20,33], which is also in closer agreement with the preheat values inferred by Christopherson *et al.* [19]. The narrower emission angle will be used throughout the rest of this paper. The larger the emission angle the more important refluxing is as a larger fraction of hot electrons will miss the target.

This paper presents results from a semi-empirical kinetic 3D Monte-Carlo transport model for hot electrons which is run inline with a radiation-hydrodynamics code (Odin). The hot-electron distribution was constrained by a polar direct-drive (PDD)[51–54] solid target experiment on the National Ignition Facility[55] (NIF). This experiment achieved $I \simeq 3\times10^{15}\mathrm{W/cm^2}$ intensities, density scale lengths $L_n \simeq 600$nm and electron temperatures $T_e \simeq 2.5$keV close to the conditions predicted in SI (see Table II). The experiment was carried out with a spherical target and PDD beam geometry as expected for SI (on the NIF) removing the geometric limitations of previous experiments[32,43,44]. It was found in simulation of the solid target direct drive NIF experiment that hot electrons change the shock timing due to deeper target penetration (than the laser) and lead to a modified density profile featuring a larger radius ablation front and a single shock front (in comparison a simulation without hot electrons predicts two separate shocks). When applied to the SI implosion the hot electron population is simulated to have a negative impact on performance, reducing peak areal density by $\sim 35\%$. In addition, features similar to those seen in simulations of the solid target experiment were observed, such as a modified shock timing and smaller in-flight-aspect-ratio (IFAR). These features contributed to the degradation in performance however the hot electron preheat was the most significant limiting factor. In the following sections the model will be described, then the experimental setup, the free parameters will be listed and how they were constrained. The model was then applied to a SI simulation and the impacts are compared to a simulation without the hot-electron population.

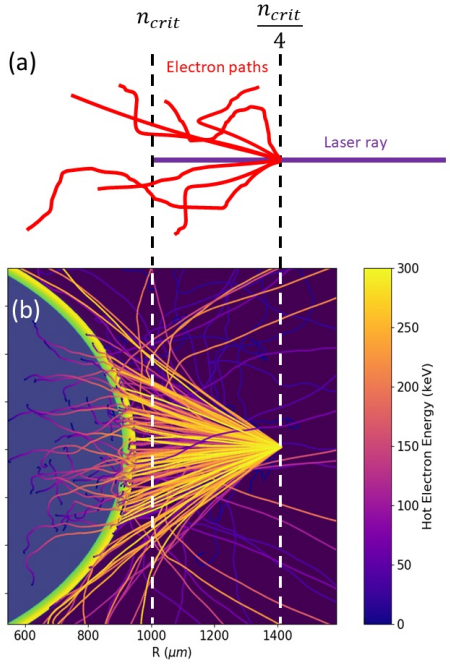

FIG. 1. (a) Schematic showing how hot electrons are generated at the $0.25n_c$ surface in Odin (b) Simulation output showing electron paths scattering and energy deposition generated from a single simulated laser ray. In (b) the colour scale refers to the hot electron energy along the path, and it is overlaid on a density plot of the NIF experimental target, the density is shown without a colour scale.

II. DESCRIPTION OF HOT ELECTRON MODEL

Figure 1 (a) gives a schematic representation of how hot electrons are transported in this model. The Odin code is a 2D radiation-hydrodynamic, arbitrary Lagrangian-Eulerian code which is run in polar coordinates. The laser drive is modelled via purely radial rays which deposit energy via inverse bremsstrahlung until they reach the quarter critical surface ($n_c/4$) at which point if the intensity is above a threshold they transfer energy into hot electrons and lose energy to SRS scattering. Any laser energy reaching the ray-turning point is deposited as thermal energy. A drive reduction multiplier is applied to the experimental laser powers before the rays are initialised.

The hot-electron particle tracking is modelled in 3D by rotating the 2D Odin grid. Hot electrons are emitted in a solid angle (Ω_h) centred parallel to ray propagation. Hot electrons are sampled from a thermal distribution. The emission angle of the electrons is randomly and uniformly distributed within the solid angle. Each electron follows a path based on the stopping and scattering formula from Berger *et al.* [56], Davies [57] and Robinson *et al.* [58]. When the hot electrons are generated, half the energy taken from the ray is put in the hot electron population ($\eta_{n_c/4}$) and the other is discarded from the simulation to account for the energy loss due to scattered SRS light. Figure 1 (b) shows a density plot of a solid target (without colour scale) with the hot electron paths overlaid. In the simulation both the emission solid angle ($\Omega_h \simeq 1.8$sr) and the size of the target viewed from the quarter critical surface $\Omega \simeq 1.2$sr are similar, in addition, the target is "thick" meaning the majority of hot electrons are stopped if incident upon it. In these simulations, we disregard the reflux population.

III. NATIONAL IGNITION FACILITY POLAR DIRECT DRIVE, SOLID TARGET EXPERIMENT

A. Experimental Setup

The method described above includes free parameters for both the hydrodynamic and hot electron models. The aim of the NIF solid target experiment (N190204-002) is to constrain these free parameters in an environment as similar to SI as possible (calibrate the simulations) but to have the benefit of a solid target for more accurate shock tracking. The experiment consists of a 1100μm radius solid target being illuminated by 184 beams in a PDD configuration. The central 1000μm is deuterated plastic (CD) and the outer 100μm is plastic (CH). A zinc backlighter is illuminated by 2 quads to give radiographic information of shock timing[59], used when constraining the hydrodynamic simulations. The FFLEX diagnostic[60] is used to measure hot electron induced bremsstrahlung x-rays, from which the hot electron population's temperature $T_h = 55 \pm 2$keV, and total energy $E_h = 35 \pm 7$kJ, is inferred[61] (the FABS diagnostic[62] indicates that SRS is the dominant cause of the hot electrons[27]). The FFLEX diagnostic is shielded from the zinc backlighter using a gold disc. The experimental laser pulse shape can be seen in Figure 2 (b) as the dashed black line. It reaches a peak power of 350TW and a peak intensity (calculated at initial target radius) of 3.0×10^{15}Wcm^{-2}. The FFLEX diagnostic was calibrated for hot electrons using a 3D Maxwellian[61] so that distribution is used throughout the simulations to best reflect the energies observed by the diagnostic.

B. Simulations to Match Observations

The experiment features a low intensity ramp used to create the ablation-plasma density scale length and temperatures anticipated in SI followed by a high intensity peak. LPI are expected to occur most during the high intensity peak $I > 10^{15}$W/cm^2 so when the experiment is simulated hot electrons and the SRS multiplier are only applied during this part of the laser pulse (supported by observations from the FFLEX diagnostic, and the FABS diagnostic[62]). The solid black line in Figure 2 (b) corresponds to the simulation laser energy absorbed, once the loss multipliers are applied (multipliers are the only loss mechanism since all the laser energy remaining in the ray is deposited into thermal electrons at critical density). The drive reduction multiplier is 0.6 applied through-

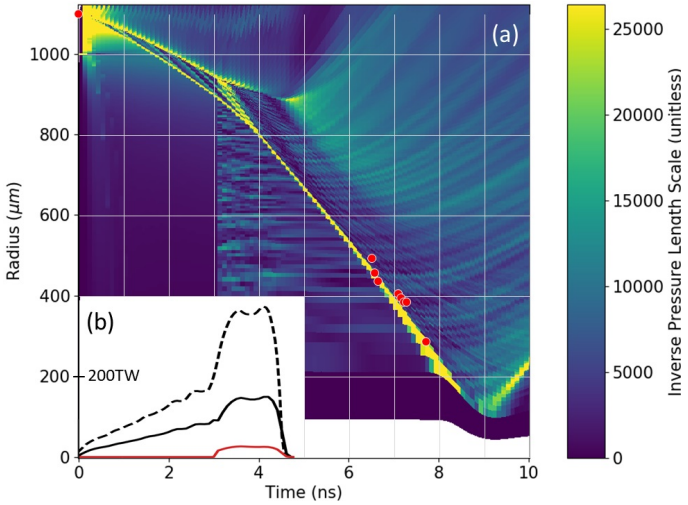

FIG. 2. (a) Inverse pressure length scale[9] ($|d\ ln(P)/dr|$) showing the shock propagation in the NIF solid target simulation (N190204-002). Red circles show the experimental shock timing extracted using x-ray radiography[59]. (b) The dashed black line is the experimental incident laser power, the solid black line is the reduced laser power to account for drive inefficiencies such as refraction, CBET, and SRS scattered light. The red solid line is the hot-electron power, equivalent to 35kJ in total energy.

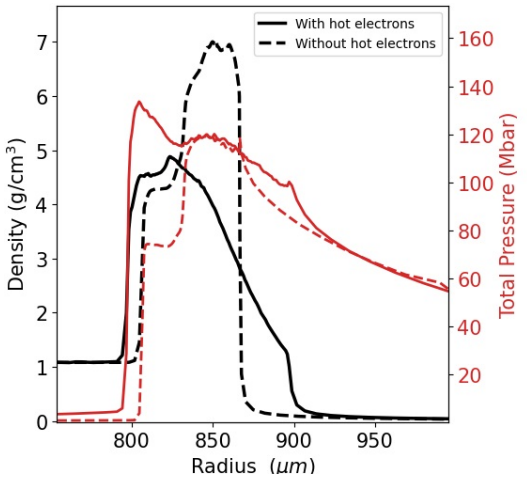

FIG. 3. A comparison of the density profile (black) and pressure profile (red) for simulations with (solid) and without (dashed) hot electrons. The snapshots show the simulations 4.0ns after the start of the laser drive. At the time of the snapshots, $\simeq 1\%$ of the hot electron energy is deposited ahead of the first shock ($R < 790\mu$m radius), $\simeq 60\%$ is deposited between the first shock and ablation front ($790 < R < 900\mu$m) and $\simeq 80\%$ is deposited within the quarter critical surface ($R < 1500\mu$m).

out the pulse (40% of laser energy removed before the ray is launched).

Figure 2 (a) shows the experimental shock timing and the close match achieved by a simulation using the parameters listed in Table I including the effect of hot electrons. The laser drive multiplier and flux limiter are chosen to match the shock timing shown in Figure 2 (a). The hot electron emission solid angle (Ω_h) is constrained by PIC simulation[33]. The hot electron conversion fraction at the quarter critical density ($\eta_{n_c/4}$) is selected to deposit the 35kJ observed by FFLEX and the hot electron population's temperature (T_h) is also constrained by the FFLEX diagnostic.

flux limiter	drive multiplier	T_h	$\eta_{n_c/4}$	Ω_h
0.06	0.6	55 keV	0.2	1.8 sr

TABLE I. Simulation parameters constrained by matching observations in the NIF directly driven solid target experiment (N190204-002). The parameters listed are, the multiplier for the electron thermal conduction flux limiter, the drive multiplier for the simulated laser pulse, the hot electron population temperature (T_h), the fraction of laser energy converted from laser to hot electrons at the quarter critical surface ($\eta_{n_c/4}$), and the solid angle over which the hot electrons are emitted (Ω_h).

Displayed in Figure 3 are snapshots at 4.0ns from the simulations of the NIF solid target experiment (N190204-002). The snapshots show the comparison of two simulations one with hot electrons shown by the solid lines, and one without hot electrons shown as the dashed lines, other than this the simulations' setup and multipliers are identical. The energy allocated to hot electrons is modified using the SRS multiplier. The SRS multiplier applied to a ray at the quarter critical density is 0.6 for simulations with hot electrons (20% discarded as scattered light and 20% put into the hot electron population, listed in Table I as the fraction $\eta_{n_c/4} = 0.2$) and 0.8 for the simulation without hot electrons (20% of the ray energy removed from the simulation as scattered light). The solid red line in Figure 2 (b) gives the simulated power deposited by hot electrons (equivalent to an energy of 35kJ which matches the experimental observations of the FFLEX diagnostic).

In Figure 3 two separate shock fronts are seen only in the simulation without hot electrons. The cause is the change from low intensity ramp to a steeper ramp at 3.0ns in the laser pulse (Figure 2 (b)). The second shock travels faster and the two will coalesce (at 5.0ns). In the simulation with hot electrons, the hot electrons penetrate deeper into the target than the laser and deposit their energy beyond the ablation front. The hot electrons are able to support the shock front created by the low intensity ramp leading to only one shock front.

At 4.0ns, shown in Figure 3, the difference in location of peak pressure between the two simulations is $\simeq 30\mu$m. The shocks travel at $\simeq 300\mu$m/ns (relative to a laboratory rest frame) giving a shock timing difference at 4.0ns of $\simeq 0.1$ns. This gap will extend to $\simeq 0.3$ns ($\simeq 90\mu$m) by 5.0ns when the two shocks (seen only in the simulation without hot electrons) coalesce. After the shocks coalesce, the difference in shock timing between the two simulations remains constant at $\simeq 0.3$ns. This is because the shocks' velocity is similar in each simulation from 5.0ns onwards. It can be inferred that it is the penetration depth of the hot electrons which has changed the timing of the first shock. Once the two shocks, in the simulation without hot electrons, have coalesced (at 5.0ns) both

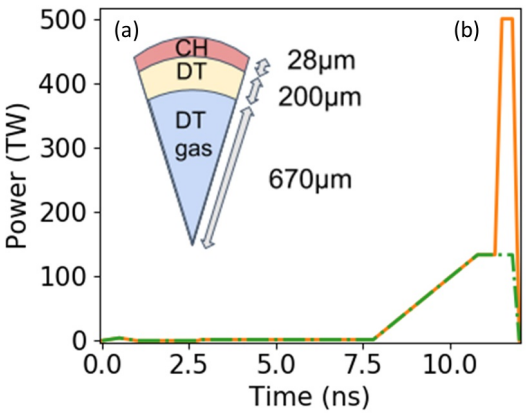

FIG. 4. (a) A schematic section of the target used in the SI implosion simulation. The capsule shell features a plastic outer layer (CH) and a DT ice inner layer, with a DT gas filled core. It is based on a design in Atzeni *et al.* [63]. (b) The laser power for SI (orange, solid line) and the laser power for the simulation without a SI spike (green, dash-dot line) which is used for performance comparison in Figure 5.

simulations have the same shock pressure and shock velocity indicating a similar overall drive efficiency. In Figure 3, preheat is visible as an increase in pressure at, $R < 790\mu$m however it has less of an impact on the shock pressure (the absolute difference in pressure ahead and behind the shock) than the effect of the hot electron energy deposited behind the shock front at $790 < R < 900\mu$m. For this reason it is stated that hot electron penetration, not preheat or drive efficiency, has changed the shock timing.

Figure 3 also demonstrates that the volumetric heating of the target by the hot electrons leads to a reduced ablator density and increased ablation front density scale length. In an implosion, this will lead to a lower in-flight-aspect-ratio (IFAR). IFAR is the ratio of initial target radius (R_i) to the minimum in-flight width of the shell wall (Δ), IFAR $= \mathrm{R_i}/\Delta$ and is a key metric for implosion efficiency[9]. This result could not be obtained with kinetic simulation of mono-energetic hot electrons.

The NIF solid target experiment (N190204-002) has been simulated and observations matched, constraining the parameters shown in Table I. The calibrated parameters can now be applied to a SI simulation.

IV. NEAR IGNITION SCALE SIMULATIONS OF SHOCK IGNITION

A. Implosion Setup

The SI capsule design is shown in Figure 4 in addition to two of the laser pulse shapes simulated. The design is based on Atzeni *et al.* [63]. However, a larger implosion velocity $V_i = 330$km/s and a larger adiabat were used (minimum adiabat at peak velocity $\alpha_{min} = 2.5$ and a fuel averaged adiabat at peak velocity $\alpha_{ave} = 3.5$) due to evidence of experimental limitations of implosions with low adiabats[12]. The use of higher adiabats results in a much lower predicted yield than most SI investigations[4,7], for this implosion the direct comparison is Atzeni *et al.* [63] which used an adiabat of $\alpha_{ave} \simeq 1.6$ and achieved a gain of $G > 50$. For the simulations presented in this paper the implosions fall short of the ignition threshold having a similar areal density and hotspot temperature (the metric of performance often used sub-ignition) to scaled versions of the current best direct drive implosions[15,64]. Using a larger adiabat means the results should be more experimentally reproducible, and there is evidence suggesting higher adiabat implosions are less susceptible to preheat[19]. The laser pulse shape requires $<$ 1MJ of laser energy and power $<$ 500TW, meaning this design is accessible by the current generation of laser facility.

The parameter calibration is only accurate if the plasma conditions are similar between the NIF solid target experiment and the SI simulation. Table II gives details of the plasma conditions simulated in the case of the experiment and SI implosion for comparison. The laser pulse shape, target size and resultant plasma conditions are similar so the inferred impact of hot electrons on SI represents an acceptable extrapolation. A notable difference between the simulations is target convergence. The SI capsule is half of its initial radius during the high intensity pulse while the NIF solid target is approximately the same radius. The convergence would likely have a negative impact on the laser coupling (absorbed over emitted laser energy, E_{Labs}/E_L) reducing it further. This means $E_L = 542$kJ is an underestimate for the laser energy required to drive such an implosion, and $542\text{kJ} < E_L < 1000$kJ is likely.

Target convergence and a less energetic high intensity pulse ($> 1.0 \times 10^{15}\mathrm{Wcm^{-2}}$), compared to the NIF experiment (N190204-002), are the main reasons for the difference in total absorbed hot electron energy (E_h) between the two simulations shown in Table II. The NIF solid target experiment, $E_h = 35$kJ, shows almost triple the energy deposited by hot electrons compared to the SI simulation $E_h = 13$kJ. Despite the lower total energy absorbed the SI implosion features more preheat (E_{h1} in Table II) due to lower areal density between the ablation front and the shock front. Preheat was defined as heating in the unshocked material for the NIF solid target experiment but in the case of the SI implosion all material is shocked (due to the picket pulses) so it is defined as heating ahead of the ignitor shock. The difference in definition also contributes to the difference in E_{h1} seen in Table II.

For shock ignition, the target cannot be assumed to be "thick", stopping the majority of hot electrons incident (the NIF solid target experiment simulations demonstrated this property). Hot electron reflux is not simulated. The fraction of hot electron energy which reaches the edge of the corona ($E_{reflux}/(E_h + E_{reflux})$) is larger for SI than for the solid target due to the solid angle the target makes when viewed from the quarter critical surface (which is $\Omega \simeq 0.67$ for SI and $\Omega \simeq 1.2$ for the NIF experiment (N190204-002)). Due to the time of flight, it is likely that the reflux population (E_{reflux}) does not play a role in the implosion except as wasted drive energy. The distance to the coronal edge, where refluxing occurs, during

Simulation	I	E_L	E_{Labs}	E_h	E_{h1}	n_c		$n_c/4$				E_{reflux}
						R	E_{h2}	R	E_{h3}	L_n	T_e	
Experiment	$3.0e15\mathrm{Wcm}^{-2}$	783 kJ	375 kJ	35 kJ	0.3kJ	1100μm	21kJ	1500μm	28kJ	500μm	2.5 keV	10kJ
Shock ignition	$5.0e15\mathrm{Wcm}^{-2}$	542 kJ	270 kJ	13 kJ	0.7kJ	500μm	7.5kJ	1000μm	10.4kJ	500μm	3.0 keV	13kJ

TABLE II. List of simulated parameters for the NIF solid target experiment and for a SI implosion. The peak laser intensity estimated using the peak power at the initial target radius (I), the laser energy emitted (E_L), the laser energy absorbed after multipliers (E_{Labs}), the total hot electron energy absorbed (E_h), and the total amount of hot electron energy absorbed ahead of the last shock (E_{h1}, approximation of preheat). The radius of the critical surface during the high intensity pulse (R) and the amount of hot electron energy deposited within the critical surface (E_{h2}). The radius of the quarter critical surface during the high intensity pulse (R) and the amount of hot electron energy deposited within the quarter critical surface $< R$ (E_{h3}, energy that contributes to shock support), the density scale length (L_n), and the electron temperature (T_e). The amount of hot electron energy that reaches the edge of the corona (E_{reflux}, wasted drive energy).

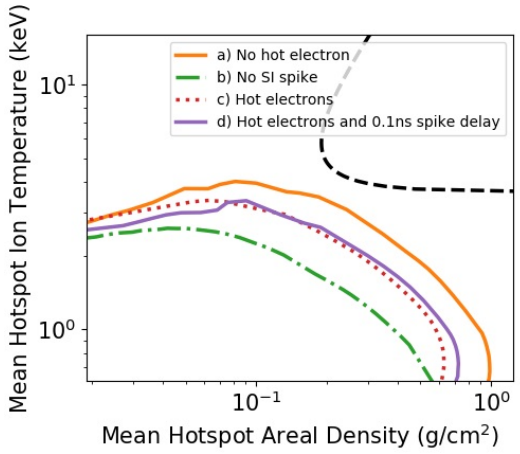

FIG. 5. Coloured lines give the hotspot thermodynamic paths using the hotspot definition $T_{edge} = \frac{T_i}{10}$ where T_i is the central temperature and T_{edge} defines the temperature at the edge of the hotspot[20]. The isobaric ignition criteria is displayed as a dashed black line[10]. The other lines correspond to four simulations, two simulated with hot electrons (red, dotted and purple, solid lines) and two that were not (green, dash-dotted and orange, solid lines). Three of the four simulations are SI, all except the green dash-dotted line labelled as "No SI spike". In this case, the laser pulse is the same except it maintains a plateau in laser power rather than a late time spike (see Figure 4). Closest to ignition is SI simulated without the impact of hot electrons (orange, solid line). The red, dotted line uses the same SI laser pulse shape (see Figure 4) but additionally models the impact of hot electrons. The purple, solid line's pulse was optimized with the effect of hot electrons, its shock spike has been delayed 0.1ns by maintaining the plateau power for longer.

the high intensity pulse is $\simeq$ 10mm, at 10% the speed of light a return journey for the fastest hot electron along the most direct path would take $\simeq$ 700ps at which point the shock collision would have already occurred, with bang-time $\simeq$ 300ps later.

B. Implosion Analysis

Figure 5 shows the impact of hot electrons on SI implosions. The baseline performance of a conventional central hotpot implosion is demonstrated by the green dash-dotted line. In the other three simulations performance is improved by adding a late-time SI spike (as shown in Figure 4). By putting extra laser energy into the SI spike, rather than the pulse's plateau, one can increase the hotspot temperature without significantly modifying the shell's IFAR or peak velocity. This demonstrates the ability of SI to increase the design space of hydrodynamically stable implosions.

The best performing implosion in Figure 5 is shock ignition simulated without hot electrons (orange-solid line) in which both hotspot ion temperature and peak areal density are approximately double that seen in the baseline case (green dash-dotted line). When a hot electron population is added to the simulations, implosion performance is reduced by 35% (as measured by peak areal density). The 35% can be compared to the $10-40$% degradation seen in direct drive conventional hotspot implosions due to hot electrons[19]. The amount of degradation is similar despite the larger SI hot electron population cumulative energy because the population is generated in the late stages of the implosion. At late times, the shell has a larger areal density, and the shell has a higher adiabat, in addition more hot electrons miss the target due to convergence. It is also likely that the two plasmon decay (TPD) hot electrons seen at lower intensities (used for conventional hotspot implosions) have a higher temperature and are thus more likely to cause preheat[27]. It is clear that hot electrons pose a threat to implosion performance for both types of direct drive fusion, so mitigation strategies are key. Delaying the SI laser spike by 0.1ns (hence the ignitor shock timing) mitigated the negative impact of the hot electrons from 35% to 25% reduction in peak areal density. The optimization in performance can be seen in Figure 5 as the difference between the red-dotted and the purple-solid line, although much of the benefit (improved compression) is in the cold fuel not the hotspot which is plotted.

The laser pulse shape that was optimized with hot electrons is compared to the simulation without hot electrons in Figure 6. The maximum pressure of the shock is similar despite $\simeq$ 20% of the laser spike going into a hot electron population. This result is similar to that seen in the NIF solid target simulation (in Figure 2). The minimum pressure ahead of the shock is increased from $\simeq$ 0.3Gbar to $\simeq$ 0.6Gbar due to hot electron preheat. The preheat, not the loss of drive, leads to the majority of the degradation in performance. The doubling

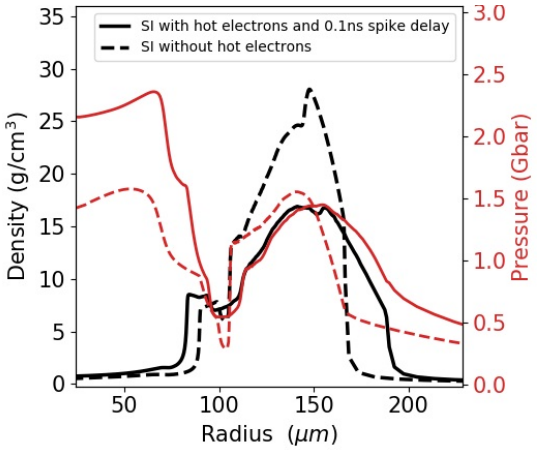

FIG. 6. Density (black) and pressure (red) achieving optimal shock timing for a simulation with (solid) and without (dashed) hot electrons. The figure displays the simulations at 12.1ns after the start of the laser pulse, this is the moment before the outgoing shock collides with the incoming igniter shock at $\simeq 100\mu$m. The simulation with hot electrons has its SI spike delayed by 0.1ns. By changing the laser pulse shape (delaying the shock spike by 0.1ns), the shock timing matches the shock timing for the simulation without hot electrons. For reference, the shock travels $\simeq 30\mu$m in 0.1ns. At $R < 200\mu$m approximately 2kJ of hot electron energy was deposited. Some of that energy aided in driving the shock but some can be seen as preheat in the increased hotspot pressure (at $R < 100\mu$m).

of pressure is visible throughout the hotspot and shell which is in line with the doubling of adiabat observed at peak velocity from $\alpha_{min} = 2.5$ to $\alpha_{min} = 6$. Figure 6 also shows the expansion of the outer edge of the target (ablation front) due to the hot electrons depositing energy within the shell. This decreases the IFAR and reduces the efficiency of energy transfer to the hotspot. A similar expansion of the target's ablation front is visible in the NIF solid target simulation (in Figure 2). An additional effect is a lower shock pressure gradient when simulated with hot electrons due to the volumetric energy deposition of the thermal distribution of hot electrons around the location that the shock forms. This shallower shock pressure gradient will result in a weaker shock collision and energy dissipation as the shock travels, which contributes to the reduction in performance and the increased adiabat seen when hot electrons are included in the simulation.

In the NIF solid target experiment, there is uncertainty in the measurement of the hot electron population. By using FFLEX and FABS diagnostic in combination, the experiment represents the state of the art in LPI diagnosis. The experiment was carried out at the National Ignition Facility which is one of few facilities capable of creating SI conditions in a near spherical geometry (not planar or conic target), limited by polar configuration of the ports. It is thought that beam geometry plays a large role in many LPI. Despite this, the results reflect a single experiment and are thus vulnerable to the variability observed in ICF experiments. Furthermore, while the conditions in the NIF solid target experiment are close to SI, the experimental laser intensity is $3 \times 10^{15}\mathrm{W/cm^2}$ which is lower than that used in our simulations ($1 \times 10^{16}\mathrm{W/cm^2}$, see Table II). At the experimental intensities, TPD is expected to play a larger role and may increase the observed hot electron temperature and reduce the hot electron energy deposited. The quarter critical surface is the region where absolute backscattered SRS occurs and so it is used as the launch site for the hot electrons in our simulations, however there is evidence that SRS occurs at a range of densities below quarter critical as well[27,32,36,40]. Given the experimental evidence and PIC simulations[33], the most probable values for the hot electron population were used in each case, but these are scaled from the NIF experiment and different laser intensities may generate a different hot-electron distribution.

For a thermal distribution of hot electrons, we find higher temperatures more disruptive to the implosion and lower temperatures behave more similarly to simulations that ignore the impact of hot electrons. It is worth noting that even without the impact of hot electrons, there is the impact of lost drive energy of the LPI scattered light. If the hot electrons are emitted further from the target at densities less than quarter critical, hot electron reflux plays a larger role. It is likely that more of the drive energy is wasted in the corona due to a larger fraction of hot electrons missing the target, but there will also be less target preheat, so the implosion is likely to perform slightly better.

V. DISCUSSION AND CONCLUSIONS

This paper presents an investigation of the impacts of hot electrons on a SI implosion and a design that may possible on current facilities. The SI simulations were constrained by an easier to diagnose solid target experiment undertaken on the NIF where the plasma conditions and laser pulse shape were similar to that of SI. The 25% reduction in peak areal density is an indication that hot electrons play a key role in SI. Similar performance reductions are observed in conventional hotspot ignition[19] meaning that SI still offers a useful method to expand the design space for direct drive implosions. When designing future direct drive or PDD campaigns this work gives evidence that the baseline performance of a conventional central hotpot ignition implosion can be improved without significantly impacting the implosion velocity a key marker of hydrodynamic stability however hot electrons will preheat the cold fuel and reduce the IFAR unless fully mitigated.

Significantly, the adiabat used in this investigation was higher than in most SI ignition simulations. A higher adiabat reduces the possible performance of an implosion but adheres to the empirical observations in several experimental campaigns on the NIF and the OMEGA facility[12–15]. The larger adiabat not just makes the design more robust to hydrodynamic instabilities but also to laser-plasma instabilities as the resulting hot electrons are predicted to have a lesser impact on high adiabat implosions[19]. This latter point may be under represented in the literature investigating the benefits of high adiabat implosions due to the difficulties in simulating LPI and hot electrons.

This paper demonstrates that shock retiming can be used

to reduce the negative impact of hot electrons, but additional strategies such as thicker targets[20], doping the ablator[65], shorter wavelength and broadband lasers[66] will be key for attempts at direct drive ignition.

The subject of hot electron generation and source characteristics is led by experiment. At present there is limited data and significant measurement uncertainty for SI conditions. The simulations in this work uses new data to characterize the hot electron population and to classify its impacts on SI relevant target designs. It is clear there is need for further experiments to reduce the uncertainty as the potential impact on implosion performance is significant. Proposed facilities with higher experimental repetition rate will improve the statistical significance of future LPI and hot electron measurements. In addition, experimental diagnosis of the fraction of hot electron energy that is deposited on the inner surface of the shell (which can be achieved using a doped target) will be essential as it is this preheat which has the most detrimental effect on the implosion. The measurement will give key insight to experimentally constrain the hot electron emission angle and reflux behaviour.

VI. ACKNOWLEDGEMENTS

This work was carried out within the framework of the UKRI, Engineering and Physical Sciences Research Council (EPSRC) under grants EP/P026796/1, EP/P023460/1, EP/P026486/1 and EP/L01663X/1. This work has been carried out within the framework of the EUROfusion Consortium and has received funding from the Euratom research and training programme 2019-2021 and 2021-2024 under grant agreement No. 633053. The views and opinions expressed herein do not necessarily reflect those of the European Commission. The involved teams have operated within the framework of the Enabling Research Project: ENR-IFE.01.CEA “Advancing shock ignition for direct-drive inertial fusion". Part of this work was performed at the Laboratory for Laser Energetics for the U.S. Department of Energy National Nuclear Security Administration under Grant No. DE-NA 0003856.

[1] V. Shcherbakov, “Ignition of a laser-fusion target by a focusing shock wave,” Sov. J. Plasma Phys.(Engl. Transl.);(United States) **9** (1983).

[2] V. Shcherbakov, “Of the expediency of making double-pulse lasers for laser thermonuclear fusion,” Voprosy Atomnoj Nauki i Tekhniki. Yaderno-Fizicheskie Issledovaniya (2003).

[3] A. Aleksandrova, N. Popov, and V. Shcherbakov, “A criterion for dt gas thermonuclear ignition by a focusing spherical shock wave,” Voprosy Atomnoj Nauki i Tekhniki (2003).

[4] R. Betti, C. Zhou, K. Anderson, L. Perkins, W. Theobald, and A. Solodov, “Shock ignition of thermonuclear fuel with high areal density,” Physical review letters **98**, 155001 (2007).

[5] W. Theobald, R. Betti, C. Stoeckl, K. Anderson, J. Delettrez, V. Y. Glebov, V. Goncharov, F. Marshall, D. Maywar, R. McCrory, *et al.*, “Initial experiments on the shock-ignition inertial confinement fusion concept,” Physics of Plasmas **15**, 056306 (2008).

[6] X. Ribeyre, G. Schurtz, M. Lafon, S. Galera, and S. Weber, “Shock ignition: an alternative scheme for hiper,” Plasma Physics and Controlled Fusion **51**, 015013 (2008).

[7] L. J. Perkins, R. Betti, K. LaFortune, and W. Williams, “Shock ignition: A new approach to high gain inertial confinement fusion on the national ignition facility,” Physical review letters **103**, 045004 (2009).

[8] J. Nuckolls, L. Wood, A. Thiessen, and G. Zimmerman, “Laser compression of matter to super-high densities: Thermonuclear (ctr) applications,” Nature **239**, 139–142 (1972).

[9] R. Craxton, K. Anderson, T. Boehly, V. Goncharov, D. Harding, J. Knauer, R. McCrory, P. McKenty, D. Meyerhofer, J. Myatt, *et al.*, “Direct-drive inertial confinement fusion: A review,” Physics of Plasmas **22**, 110501 (2015).

[10] S. Atzeni and J. Meyer-ter Vehn, *The physics of inertial fusion: beam plasma interaction, hydrodynamics, hot dense matter*, Vol. 125 (OUP Oxford, 2004).

[11] M. Tabak, D. Munro, and J. Lindl, “Hydrodynamic stability and the direct drive approach to laser fusion,” Physics of Fluids B: Plasma Physics **2**, 1007–1014 (1990).

[12] J. Lindl, O. Landen, J. Edwards, E. Moses, and N. team, “Review of the national ignition campaign 2009-2012,” Physics of Plasmas **21**, 020501 (2014).

[13] A. Zylstra, A. Kritcher, O. Hurricane, D. Callahan, K. Baker, T. Braun, D. Casey, D. Clark, K. Clark, T. Döppner, *et al.*, “Record energetics for an inertial fusion implosion at nif,” Physical Review Letters **126**, 025001 (2021).

[14] A. Kritcher, A. Zylstra, D. Callahan, O. Hurricane, C. Weber, J. Ralph, D. Casey, A. Pak, K. Baker, B. Bachmann, *et al.*, “Achieving record hot spot energies with large hdc implosions on nif in hybrid-e,” Physics of Plasmas **28**, 072706 (2021).

[15] C. Williams, R. Betti, V. Gopalaswamy, and A. Lees, “High yields in direct-drive inertial confinement fusion using thin-ice dt liner targets,” Physics of Plasmas **28**, 122708 (2021).

[16] J. Trela, W. Theobald, K. Anderson, D. Batani, R. Betti, A. Casner, J. Delettrez, J. Frenje, V. Y. Glebov, X. Ribeyre, *et al.*, “The control of hot-electron preheat in shock-ignition implosions,” Physics of Plasmas **25**, 052707 (2018).

[17] K. Anderson, R. Betti, P. McKenty, T. Collins, M. Hohenberger, W. Theobald, R. Craxton, J. Delettrez, M. Lafon, J. Marozas, *et al.*, “A polar-drive shock-ignition design for the national ignition facility,” Physics of Plasmas **20**, 056312 (2013).

[18] J. Myatt, J. Zhang, R. Short, A. Maximov, W. Seka, D. Froula, D. Edgell, D. Michel, I. Igumenshchev, D. Hinkel, *et al.*, “Multiple-beam laser–plasma interactions in inertial confinement fusion,” Physics of Plasmas **21**, 055501 (2014).

[19] A. Christopherson, R. Betti, C. Forrest, J. Howard, W. Theobald, J. Delettrez, M. Rosenberg, A. Solodov, C. Stoeckl, D. Patel, *et al.*, “Direct measurements of dt fuel preheat from hot electrons in direct-drive inertial confinement fusion,” Physical Review Letters **127**, 055001 (2021).

[20] A. Colaïtis, X. Ribeyre, E. Le Bel, G. Duchateau, P. Nicolaï, and V. Tikhonchuk, “Influence of laser induced hot electrons on the threshold for shock ignition of fusion reactions,” Physics of Plasmas **23**, 072703 (2016).

[21] W. Shang, R. Betti, S. Hu, K. Woo, L. Hao, C. Ren, A. Christopherson, A. Bose, and W. Theobald, “Electron shock ignition of inertial fusion targets,” Physical review letters **119**, 195001 (2017).

[22] R. Betti, W. Theobald, C. Zhou, K. Anderson, P. McKenty, S. Skupsky, D. Shvarts, V. Goncharov, J. Delettrez, P. Radha, *et al.*, “Shock ignition of thermonuclear fuel with high areal densities,” in *Journal of Physics: Conference Series*, Vol. 112 (IOP Publishing, 2008) p. 022024.

[23] R. Nora, R. Betti, K. Anderson, A. Shvydky, A. Bose, K. Woo, A. Christopherson, J. Marozas, T. Collins, P. Radha, *et al.*, “Theory of hydroequivalent ignition for inertial fusion and its applications to omega and the national ignition facility,” Physics of Plasmas **21**, 056316 (2014).

[24] W. Theobald, R. Nora, W. Seka, M. Lafon, K. Anderson, M. Hohenberger, F. Marshall, D. Michel, A. Solodov, C. Stoeckl, *et al.*, “Spherical strong-shock generation for shock-ignition inertial fusion,” Physics of Plasmas **22**, 056310 (2015).

[25] P. Nicolaï, J.-L. Feugeas, M. Touati, X. Ribeyre, S. Gus’ kov, and V. Tikhonchuk, “Deleterious effects of nonthermal electrons in shock ignition concept,” Physical Review E **89**, 033107 (2014).

[26] A. Colaïtis, G. Duchateau, X. Ribeyre, Y. Maheut, G. Boutoux, L. Antonelli, P. Nicolaï, D. Batani, and V. Tikhonchuk, “Coupled hydrodynamic model for laser-plasma interaction and hot electron generation,” Physical Review E **92**, 041101 (2015).

[27] M. Rosenberg, A. Solodov, J. Myatt, W. Seka, P. Michel, M. Hohenberger, R. Short, R. Epstein, S. Regan, E. Campbell, *et al.*, “Origins and scaling

of hot-electron preheat in ignition-scale direct-drive inertial confinement fusion experiments," Physical review letters **120**, 055001 (2018).
[28]S. Gus'kov, X. Ribeyre, M. Touati, J.-L. Feugeas, P. Nicolaï, and V. Tikhonchuk, "Ablation pressure driven by an energetic electron beam in a dense plasma," Physical review letters **109**, 255004 (2012).
[29]S. Y. Gus'kov, P. Kuchugov, R. Yakhin, and N. Zmitrenko, "The role of fast electron energy transfer in the problem of shock ignition of laser thermonuclear target," High Energy Density Physics **36**, 100835 (2020).
[30]S. Y. Gus'kov, N. Demchenko, E. Dmitriev, P. Kuchugov, G. Vergunova, and R. Yakhin, "Fast-electron maintaining a high shock-ignition gain with a significant decrease in the laser pulse energy," Plasma Physics and Controlled Fusion **64**, 045011 (2022).
[31]S. Bel'kov, S. Bondarenko, S. Garanin, S. Y. Gus'kov, N. Demchenko, N. Zmitrenko, P. Kuchugov, R. Stepanov, V. Shcherbakov, and R. Yakhin, "Features of the ignition of a laser fusion target by a converging shock wave," Journal of Experimental and Theoretical Physics **131**, 636–644 (2020).
[32]R. Scott, K. Glize, L. Antonelli, M. Khan, W. Theobald, M. Wei, R. Betti, C. Stoeckl, A. Seaton, T. Arber, *et al.*, "Shock ignition laser-plasma interactions in ignition-scale plasmas," Physical Review Letters **127**, 065001 (2021).
[33]A. G. Seaton and T. D. Arber, "Laser-plasma instabilities in long scale-length plasmas relevant to shock-ignition," Physics of Plasmas **27**, 082704 (2020).
[34]S. Baton, A. Colaitis, C. Rousseaux, G. Boutoux, S. Brygoo, L. Jacquet, M. Koenig, D. Batani, A. Casner, E. Le Bel, *et al.*, "Preliminary results from the lmj-petal experiment on hot electrons characterization in the context of shock ignition," High Energy Density Physics **36**, 100796 (2020).
[35]S. Y. Gus' kov, N. Demchenko, A. Kasperczuk, T. Pisarczyk, Z. Kalinowska, T. Chodukowski, O. Renner, M. Smid, E. Krousky, M. Pfeifer, *et al.*, "Laser-driven ablation through fast electrons in pals-experiment at the laser radiation intensity of 1–50 pw/cm2," Laser and Particle Beams **32**, 177–195 (2014).
[36]G. Cristoforetti, L. Antonelli, D. Mancelli, S. Atzeni, F. Baffigi, F. Barbato, D. Batani, G. Boutoux, F. D'Amato, J. Dostal, *et al.*, "Time evolution of stimulated raman scattering and two-plasmon decay at laser intensities relevant for shock ignition in a hot plasma," High Power Laser Science and Engineering **7** (2019).
[37]D. Batani, L. Antonelli, F. Barbato, G. Boutoux, A. Colaïtis, J.-L. Feugeas, G. Folpini, D. Mancelli, P. Nicolaï, J. Santos, *et al.*, "Progress in understanding the role of hot electrons for the shock ignition approach to inertial confinement fusion," Nuclear Fusion **59**, 032012 (2018).
[38]G. Cristoforetti, A. Colaïtis, L. Antonelli, S. Atzeni, F. Baffigi, D. Batani, F. Barbato, G. Boutoux, R. Dudzak, P. Koester, *et al.*, "Experimental observation of parametric instabilities at laser intensities relevant for shock ignition," EPL (Europhysics Letters) **117**, 35001 (2017).
[39]L. Antonelli, J. Trela, F. Barbato, G. Boutoux, P. Nicolaï, D. Batani, V. Tikhonchuk, D. Mancelli, A. Tentori, S. Atzeni, *et al.*, "Laser-driven strong shocks with infrared lasers at intensity of 1016 w/cm2," Physics of Plasmas **26**, 112708 (2019).
[40]G. Cristoforetti, S. Hüller, P. Koester, L. Antonelli, S. Atzeni, F. Baffigi, D. Batani, C. Baird, N. Booth, M. Galimberti, *et al.*, "Observation and modelling of stimulated raman scattering driven by an optically smoothed laser beam in experimental conditions relevant for shock ignition," High Power Laser Science and Engineering **9** (2021).
[41]T. Boehly, D. Brown, R. Craxton, R. Keck, J. Knauer, J. Kelly, T. Kessler, S. Kumpan, S. Loucks, S. Letzring, *et al.*, "Initial performance results of the omega laser system," Optics communications **133**, 495–506 (1997).
[42]D. Maywar, J. Kelly, L. Waxer, S. Morse, I. Begishev, J. Bromage, C. Dorrer, J. Edwards, L. Folnsbee, M. Guardalben, *et al.*, "Omega ep high-energy petawatt laser: progress and prospects," in *Journal of Physics: Conference Series*, Vol. 112 (IOP Publishing, 2008) p. 032007.
[43]S. Zhang, C. Krauland, J. Peebles, J. Li, F. Beg, N. Alexander, W. Theobald, R. Betti, D. Haberberger, E. Campbell, *et al.*, "Experimental study of hot electron generation in shock ignition relevant high-intensity regime with large scale hot plasmas," Physics of Plasmas **27**, 023111 (2020).
[44]A. Tentori, A. Colaïtis, W. Theobald, A. Casner, D. Raffestin, A. Ruocco, J. Trela, E. Le Bel, K. Anderson, M. Wei, *et al.*, "Experimental characterization of hot-electron emission and shock dynamics in the context of the shock ignition approach to inertial confinement fusion," Physics of Plasmas **28**, 103302 (2021).
[45]J. Delettrez, T. Collins, and C. Ye, "Determining acceptable limits of fast-electron preheat in direct-drive-ignition–scale target designs," Physics of Plasmas **26**, 062705 (2019).
[46]N. Sinenian, M. J. Manuel, J. Frenje, F. Séguin, C. Li, and R. Petrasso, "An empirical target discharging model relevant to hot-electron preheat in direct-drive implosions on omega," Plasma Physics and Controlled Fusion **55**, 045001 (2013).
[47]L. Volpe, D. Batani, A. Morace, and J. Santos, "Collisional and collective effects in two dimensional model for fast-electron transport in refluxing regime," Physics of Plasmas **20**, 013104 (2013).
[48]T. Pisarczyk, M. Kalal, S. Y. Gus'kov, D. Batani, O. Renner, J. Santos, R. Dudzak, A. Zaras-Szydłowska, T. Chodukowski, Z. Rusiniak, *et al.*, "Hot electron retention in laser plasma created under terawatt subnanosecond irradiation of cu targets," Plasma Physics and Controlled Fusion **62**, 115020 (2020).
[49]S. Y. Gus'kov, P. Kuchugov, R. Yakhin, and N. Zmitrenko, "Effect of 'wandering'and other features of energy transfer by fast electrons in a direct-drive inertial confinement fusion target," Plasma Physics and Controlled Fusion **61**, 055003 (2019).
[50]B. Yaakobi, A. Solodov, J. Myatt, J. Delettrez, C. Stoeckl, and D. Froula, "Measurements of the divergence of fast electrons in laser-irradiated spherical targets," Physics of Plasmas **20**, 092706 (2013).
[51]S. Skupsky, J. Marozas, R. Craxton, R. Betti, T. Collins, J. Delettrez, V. Goncharov, P. McKenty, P. Radha, T. Boehly, *et al.*, "Polar direct drive on the national ignition facility," Physics of Plasmas **11**, 2763–2770 (2004).
[52]T. Collins, J. Marozas, K. Anderson, R. Betti, R. Craxton, J. Delettrez, V. Goncharov, D. Harding, F. Marshall, R. McCrory, *et al.*, "A polar-drive–ignition design for the national ignition facility," Physics of Plasmas **19**, 056308 (2012).
[53]M. Hohenberger, P. Radha, J. Myatt, S. LePape, J. Marozas, F. Marshall, D. Michel, S. Regan, W. Seka, A. Shvydky, *et al.*, "Polar-direct-drive experiments on the national ignition facility," Physics of Plasmas **22**, 056308 (2015).
[54]P. Radha, M. Hohenberger, D. Edgell, J. Marozas, F. Marshall, D. Michel, M. Rosenberg, W. Seka, A. Shvydky, T. Boehly, *et al.*, "Direct drive: Simulations and results from the national ignition facility," Physics of Plasmas **23**, 056305 (2016).
[55]G. H. Miller, E. I. Moses, and C. R. Wuest, "The national ignition facility," Optical Engineering **43**, 2841–2853 (2004).
[56]M. Berger, M. Inokuti, H. Anderson, H. Bichsel, J. Dennis, D. Powers, S. Seltzer, and J. Turner, "Report 37," Journal of the International Commission on Radiation Units and Measurements , NP–NP (1984).
[57]J. Davies, "How wrong is collisional monte carlo modeling of fast electron transport in high-intensity laser-solid interactions?" Physical Review E **65**, 026407 (2002).
[58]A. Robinson, D. Strozzi, J. Davies, L. Gremillet, J. Honrubia, T. Johzaki, R. Kingham, M. Sherlock, and A. Solodov, "Theory of fast electron transport for fast ignition," Nuclear Fusion **54**, 054003 (2014).
[59]G. Kyrala, S. Dixit, S. Glenzer, D. Kalantar, D. Bradley, N. Izumi, N. Meezan, O. Landen, D. Callahan, S. Weber, *et al.*, "Measuring symmetry of implosions in cryogenic hohlraums at the nif using gated x-ray detectors," Review of Scientific Instruments **81**, 10E316 (2010).
[60]J. McDonald, R. Kauffman, J. Celeste, M. Rhodes, F. Lee, L. Suter, A. Lee, J. Foster, and G. Slark, "A filter-fluorescer diagnostic system (fflex) for the national ignition facility (nif)," Tech. Rep. (Lawrence Livermore National Lab., 2004).
[61]M. Hohenberger, N. Palmer, G. LaCaille, E. Dewald, L. Divol, E. Bond, T. Döppner, J. Lee, R. Kauffman, J. Salmonson, *et al.*, "Measuring the hot-electron population using time-resolved hard x-ray detectors on the nif," in *Target Diagnostics Physics and Engineering for Inertial Confinement Fusion II*, Vol. 8850 (International Society for Optics and Photonics, 2013) p. 88500F.
[62]D. Froula, D. Bower, M. Chrisp, S. Grace, J. Kamperschroer, T. Kelleher, R. Kirkwood, B. MacGowan, T. McCarville, N. Sewall, *et al.*, "Full-aperture backscatter measurements on the national ignition facility," Review of scientific instruments **75**, 4168–4170 (2004).
[63]S. Atzeni, A. Schiavi, L. Antonelli, and A. Serpi, "Hydrodynamic studies of high gain shock ignition targets: effect of low-to intermediate-mode asymmetries," The European Physical Journal D **73**, 1–10 (2019).

[64] V. Gopalaswamy, R. Betti, J. Knauer, N. Luciani, D. Patel, K. Woo, A. Bose, I. Igumenshchev, E. Campbell, K. Anderson, *et al.*, "Tripled yield in direct-drive laser fusion through statistical modelling," Nature **565**, 581–586 (2019).

[65] W. Theobald, A. Bose, R. Yan, R. Betti, M. Lafon, D. Mangino, A. Christopherson, C. Stoeckl, W. Seka, W. Shang, *et al.*, "Enhanced hot-electron production and strong-shock generation in hydrogen-rich ablators for shock ignition," Physics of Plasmas **24**, 120702 (2017).

[66] T. Lehecka, S. Bodner, A. Deniz, A. Mostovych, S. Obenschain, C. Pawley, and M. Pronko, "The nike krf laser fusion facility," Journal of fusion energy **10**, 301–303 (1991).